A Study of Electromagnetic Transient Simulations Using IEEJ's West-10 Benchmark Power System Model

Taku Noda, Hiroshi Takizawa and Takayuki Nakajima

Abstract— **Electromagnetic-transient (EMT) simulations of relatively-large power systems with generator mechanical dynamics have become quite common especially for studies of power systems including power-electronics converters. The Power and Energy Society of the Institute of Electrical Engineers of Japan (IEEJ) prepared benchmark power system models for transient stability (TS) simulations. Among those, the West-10 benchmark power system model approximately represents the long radial power system in the western part (60-Hz part) of Japan with ten generators. In this paper, the West-10 benchmark power system model is expanded and converted to an EMT model, and it is shown that the results obtained by the EMT model agree well with those obtained by the TS model in most cases. It is also found that when the dc components of fault currents are large the results obtained by those two simulation methods are different due to current zero missing of circuit breakers.**

Index Terms— **EMT simulations, IEEJ's West-10 benchmark power system model, relatively-large power systems, and stability-type simulations.**

I. Introduction

MODERN power systems utilize power-electronics converters for dc transmission, back-to-back system interconnection (frequency conversion between 50 and 60 Hz), system stabilization, and so on. Since waveform-level calculations are essential to take into account switchings in power-electronics converters, studies of power systems including power-electronics converters are now often carried out by electromagnetic transient (EMT) simulations. This trend gives further importance to EMT simulations in addition to studies of conventional phenomena such as overvoltages, inrush currents, and abnormal oscillations. Thanks to the research and development of simulation methods and also to the progress of simulation hardware (computers), EMT simulations of relatively-large power systems with generator mechanical dynamics have become quite common. The EMT simulations related to power electronics converters mentioned above and sub-synchronous resonance often involve relatively-large power systems.

T. Noda is with Electric Power Engineering Research Laboratory, CRIEPI (Central Research Institute of Electric Power Industry), 2-6-1 Nagasaka, Yokosuka, Kanagawa 240-0196, Japan (e-mail: takunoda@criepi.denken.or.jp).

H. Takizawa and T. Nakajima are with DCC (Denryoku Computing Center), 1-1-1 Manpuku-ji, Asao-ku, Kawasaki, Kanagawa 215-0004, Japan (e-mail: {taki, nakaji}@dcc.co.jp).

Paper submitted to the International Conference on Power Systems Transients (IPST2015) in Cavtat, Croatia, June 15-18, 2015.

The Power and Energy Society of the Institute of Electrical Engineers of Japan (IEEJ) prepared benchmark power system models for transient stability (TS) simulations. Among those, the West-10 benchmark power system model approximately represents the long radial power system in the western part (60-Hz part) of Japan with ten generators.

In this paper, the West-10 benchmark power system model is expanded and converted to an EMT model for the implementation in EMT simulation programs. The major differences between the EMT and the TS simulation are as follows. The EMT simulation calculates three-phase voltage and current waveforms, while the TS simulation calculates positive-sequence r.m.s. values. In addition, voltages and currents in the EMT simulation are in units of volts and amperes, while those in the TS simulation are based on the per-unit system. Therefore, all models have to be expanded and converted to three-phase waveform-based ones, and appropriate nominal voltages have to be given for all buses. Furthermore, an appropriate winding connection, such as star-delta, star-star-delta, and so on, has to be assumed for each transformer, and an appropriate grounding impedance has to be added to each neutral point.

Using the developed EMT model of the West-10 benchmark power system, simulations with various fault scenarios are carried out. It is shown in this paper that the results obtained by the EMT model agree well with those obtained by the original TS model in most cases. It is also found that when the dc components of fault currents are large, the results obtained by those two simulation methods are different due to current zero missing of circuit breakers. For the comparison with the TS results, π equivalents are used for the modeling of the transmission lines, and they are then replaced with constant-parameter line models for more practical simulation so as to discuss the impact of line modeling.

II. IEEJ's West-10 Benchmark Power System Model

The 60-Hz power system in Japan interconnects several electric power companies with 500-kV transmission lines and extends more than 1,000 km in an east-west direction. The system can roughly be considered a radial system. IEEJ's West-10 benchmark power system model, called the "West-10 Benchmark System" hereafter, approximates this radial system with ten generators. Since only the summary of the West-10 Benchmark System is given here, ref. [1] should be consulted for details.

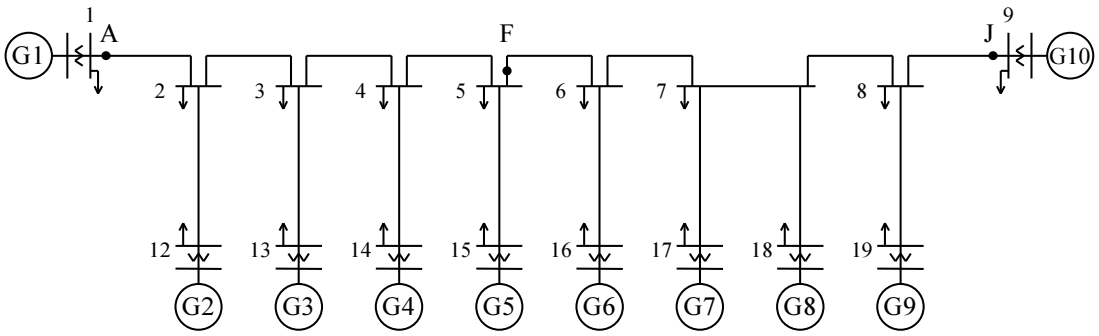

Fig. 1. One-line diagram of the West-10 Benchmark System (IEEJ's West-10 benchmark power system model).

TABLE I
GENERATOR MODEL CONSTANTS.

d-axis synchronous reactance x_d [p.u.]	1.70
q-axis synchronous reactance x_q [p.u.]	1.70
d-axis transient reactance x_d' [p.u.]	0.35
d-axis subtransient reactance x_d'' [p.u.]	0.25
q-axis subtransient reactance x_q'' [p.u.]	0.25
d-axis transient time constant T_d' [s]	1.00
d-axis subtransient time constant T_d'' [s]	0.03
q-axis subtransient time constant T_q'' [s]	0.03
armature time constant T_a [s]	0.40
armature leakage reactance x_l [p.u.]	0.225

Fig. 1 shows the one-line diagram of the West-10 Benchmark System. The system frequency is 60 Hz.

A. Generators

All of the ten generators are represented by a dq-frame-based synchronous generator model with one damper winding for each of the d and the q frame [2]. The constants of the generator models are set to the values shown in Table I. These values are typical for large-scale thermal-plant generators, and the reactance values are based on their own ratings shown in Table II (see Section II-D for the peak-load and light-load conditions). The inertia constants of all generator models are set to 7 s. Each generator model has an exciter (AVR: automatic voltage regulator) model and a turbine-governor model. The exciter model represents a rotating exciter, and its control-block diagram is shown in Fig. 2 (a). The turbine-governor model whose control-block diagram is shown in Fig. 2 (b) represents a typical turbine governor used by thermal and nuclear power plants. Each generator station is equipped with a step-up transformer whose impedance is 0.14 p.u. based on its own rating, and its tap ratio is unity.

B. Transmission Lines

The nominal voltage of all transmission lines is 500 kV. Since G1 and G10 equivalently represent interconnected neighboring systems, they are considered as substations in the discussion below. The transmission lines connecting between substations are double-circuit and their length are 100 km. The impedance of these lines is $0.0021 + j0.063$ p.u. and a half of their admittance is $j0.122$. Those connecting generator stations to substations are also double-circuit. Except the one

TABLE II
GENERATOR RATINGS.

generator	peak-load rating [MVA]	light-load rating [MVA]
G1	15,000	9,000
G2–G7, G9	10,000	6,000
G8	5,000	3,000
G10	30,000	18,000

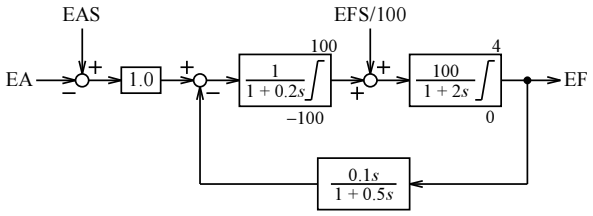

(a)

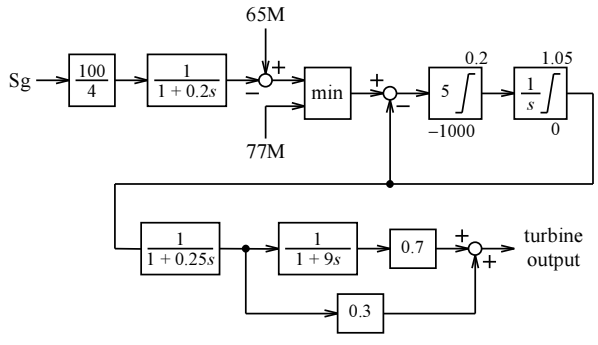

(b)

Fig. 2. Exciter and turbine-governor models. (a) Control-block diagram of the rotating exciter model, where EA and EAS are the generator terminal voltage and its initial value and EFS is the initial value of the field voltage. (b) Control-block diagram of the turbine-governor model, where Sg is the generator speed deviation. 65M and 77M are parameters related to governor-free operations and not used in the simulations in this paper.

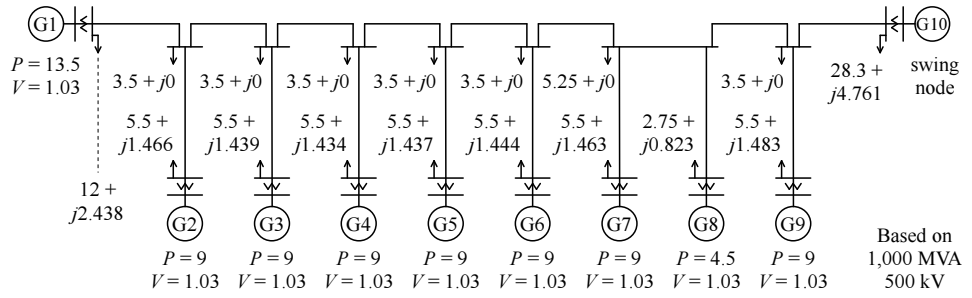

(a)

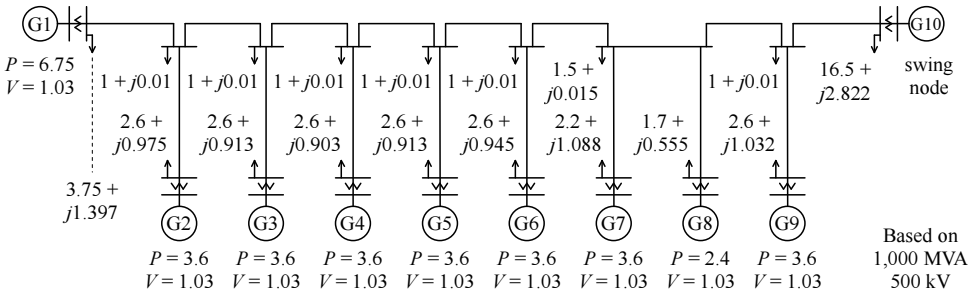

(b)

Fig. 3. Power-flow conditions. (a) Peak (daytime) load condition. (b) Light (nighttime) load condition.

connecting Bus 18 to Bus 7, their lengths are 50 km, and their impedance is $0.00105 + j0.0315$ p.u. and a half of their admittance is $j0.061$. The length of the transmission line connecting Bus 18 to Bus 7 is 100 km, and its impedance and a half of its admittance are $0.0021 + j0.063$ p.u. and $j0.122$ respectively. These line constants have been determined by assuming a bundle of four TACSR-840-mm^2 wires used for each phase. All transmission lines are modeled by single-section π equivalents.

C. Loads

The models of the loads represent the following characteristics. When the voltage V_L at the load is higher than or equal to 0.7 p.u., the active power P_L consumed by the load model shows the constant-current characteristic given by

$$P_L = P_i \left(\frac{V_L}{V_i}\right)\left(1 + \Delta f \frac{\beta}{100}\right), \tag{1}$$

where P_i and V_i are initial active-power and load-voltage values. A frequency dependence is represented with respect to the frequency deviation Δf of the load voltage with the parameter β which is set to 3.33. When V_L is smaller than 0.7 p.u., the active power shows the constant impedance characteristic given by

$$P_L = P_i \left(\frac{V_L}{V_i}\right)^2 \left(1 + \Delta f \frac{\beta}{100}\right). \tag{2}$$

This equation also represents the same frequency dependence. Regardless of the voltage value, the reactive power consumed by the load model shows the the constant-impedance characteristic

$$Q_L = Q_i \left(\frac{V_L}{V_i}\right)^2, \tag{3}$$

where Q_i is an initial reactive-power value.

TABLE III
TRANSFORMER IMPEDANCE VALUES.

generator station	peak-load	light-load
G1	$j0.00932$	$j0.01556$
G2–G7, G9	$j0.014$	$j0.02332$
G8	$j0.028$	$j0.04666$
G10	$j0.00466$	$j0.00778$

D. Power-Flow Conditions and Transformer Impedances

As the power-flow condition from which a simulation is started, the two cases, the peak (daytime) and the light (nighttime) load condition, are considered. For each case, the $P-V$ and the $P-Q$ values are respectively given to the generators and the loads as shown in Fig. 3.

The impedance values of the transformers in the generator stations are shown in Table III in p.u. based on 1,000 MVA and 500 kV. The values vary with respect to power flow conditions.

III. EMT MODELING

The simulations presented in this paper have been carried out using the EMT analysis program XTAP [3]. It uses the two-stage diagonally implicit Runge-Kutta (2S-DIRK) method for the numerical integration of dynamic circuit elements such as inductors and capacitors [4], [5]. The 2S-DIRK method does not produce fictitious numerical oscillation when an inductor current or a capacitor voltage is suddenly changed, since it is a mathematically oscillation-free algorithm. For the

solution of nonlinear circuit equations, XTAP uses a robust and efficient scheme which combines the conventional Newton-Raphson algorithm, its modified version named the biaxial Newton-Raphson algorithm, and the Katzenelson method [6]. Using this scheme, XTAP obtains the solution at each time step with a relatively small number of iterations. To start an EMT simulation from a steady state, XTAP first calculates a positive-sequence power-flow solution based on power-flow conditions given by the user, then calculates a three-phase steady-state solution based on the power-flow solution, and finally starts an EMT simulation with initializing the dynamic elements based on the preceding steady-state solution [7].

A. Generator Model

Fig. 4 (a) shows the framework of the generator model [8] used in the EMT simulations in this paper. Since the generator terminals in the abc frame are interfaced with the d- and the q-axis equivalent circuit using the dependent sources shown in Fig. 4 (b), there is no time delay in the interface between the abc and the dq frame. The voltage-controlled voltage sources that generate the dq-frame voltages are expressed by

$$\begin{array}{ll} E_{da}(t) = k\cos\theta_a\, v_a(t) & E_{qa}(t) = -k\sin\theta_a\, v_a(t) \\ E_{db}(t) = k\cos\theta_b\, v_b(t) & E_{qb}(t) = -k\sin\theta_b\, v_b(t) \\ E_{dc}(t) = k\cos\theta_c\, v_c(t) & E_{qc}(t) = -k\sin\theta_c\, v_c(t), \end{array} \tag{4}$$

where $k = \frac{2}{3}$, $\theta_a = \theta$, $\theta_b = \theta - \frac{2\pi}{3}$, $\theta_c = \theta - \frac{4\pi}{3}$, and θ is the rotor angle given by the mechanical part of the model. The current-controlled current sources that generate the abc-frame currents are expressed by

$$\begin{array}{ll} J_{ad}(t) = \cos\theta_a\, I_d(t) & J_{aq}(t) = -\sin\theta_a\, I_q(t) \\ J_{bd}(t) = \cos\theta_b\, I_d(t) & J_{bq}(t) = -\sin\theta_b\, I_q(t) \\ J_{cd}(t) = \cos\theta_c\, I_d(t) & J_{cq}(t) = -\sin\theta_c\, I_q(t). \end{array} \tag{5}$$

The electromagnetic torque is obtained by the d- and q-equivalent circuits and then passed to the generator mechanical part as the input. The differential equations describing the generator mechanical dynamics are solved using a second-order explicit Runge-Kutta method (RK2) which gives the solution at the present time step only from values at past time steps. Thus, there is no time delay associated to pass the rotor angle θ to the $abc-dq$ interface.

The nominal voltage of all generators are set to 22 kV, and each of their neutral points is grounded through a 0.1-Ω resistor representing the resistance of a generator-station grounding mesh. The model used takes into account the magnetic-flux saturation, but it is not represented in the West-10 Benchmark System. The exciter model and the turbine governor model shown in Fig. 2 are implemented as they are using the control-block library of XTAP.

B. Transformer Model

The winding connections of all transformers are assumed to be delta–star, where the primary side is delta and the secondary is star. The nominal voltage of the primary side is 22 kV, and it is connected to the generator. The secondary side whose nominal voltage is 500 kV is connected to the transmission network. The neutral point of the secondary winding is grounded through a 0.1-Ω resistor representing a generator-station grounding mesh. Although more realistic representations are possible, the leakage inductance is lumped to the primary side, and the winding resistance, the magnetizing resistance, and the magnetizing inductance are ignored. This is for comparison with TS results.

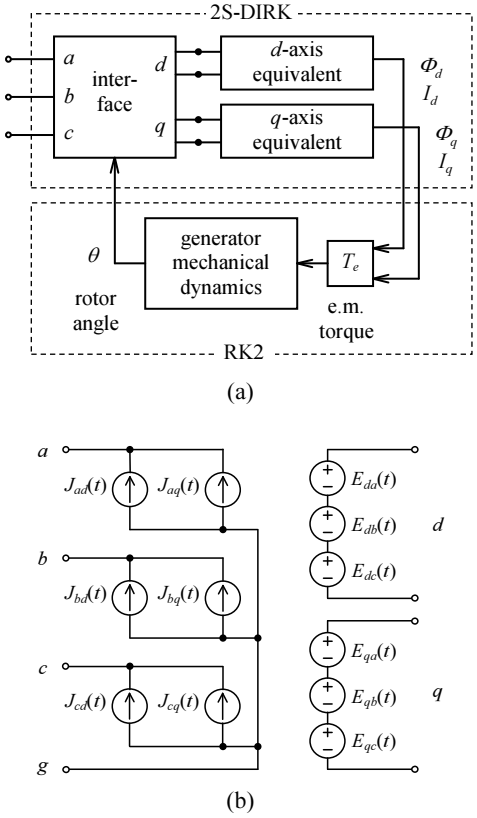

Fig. 4. Generator model used in the EMT simulations. (a) Model framework. (b) $abc-dq$ interface utilizing dependent sources.

C. Line Model

Each transmission line is represented by three sets of a single-section π-equivalent circuit with positive-sequence line constants. Again, this is for comparison with TS results. For more realistic representation, the transmission lines are represented by the constant-parameter line model [9], and its impact is discussed in Section V.

D. Load Model

The load model used basically consists of star-connected three-phase series RL branches. The resistance and the inductance value are controlled by the following algorithm. The three-phase voltages of the load model are obtained and their d- and q-axis components are calculated using the abc–$\alpha\beta$ and the $\alpha\beta-dq$ transformation so as to obtain the r.m.s. voltage. The frequency of the load voltage is obtained by a zero-crossing method. Using the r.m.s. voltage and the frequency, the active power P_L and the reactive power Q_L are calculated using (1)–(3). Then, the resistance and the inductance value of the series RL branch are calculated so that it consumes one

third of $P_L + jQ_L$, and the calculated values are reflected to the three-phase RL branches.

It is also possible to use three-phase parallel RL branches, and the determination of the RL values may be even easier in this case. However, the series RL branch is somewhat closer to the physical structure of the power network, and thus, the series branch is selected in this study.

IV. Simulation Results

EMT simulations of the West-10 Benchmark System have been carried out for the following six cases. A three-line-to-ground (3LG) fault is considered at one of the points designated by A, F, and J in Fig. 1, and the peak- and light-load conditions shown in Fig. 3 are considered as subcases for each fault-point case. The 3LG fault is considered to occur on one of the two circuits at $t = 1$ s, and the fault duration time assumed is 70 ms.

Figs. 5, 6, and 7 show the simulation results when the 3LG fault is considered at Point A, F, and J respectively. The rotor angles of G1, G3, G5, G7, and G9 are shown considering that of G10 as the phase-angle reference. The same simulation cases have also been carried out by a TS simulation program, and those results are superimposed using dashed lines in the figures. For the TS simulations in this paper, CPAT (CRIEPI's Power system Analysis Tools) which is widely used as the de-facto standard program in Japan is used [2].

In the cases where the fault occurs at A and F, the EMT simulation results agree well with the corresponding TS simulation results. In the cases of faults at J, however, the two simulation methods do not give similar results. Especially in the peak-load condition, the EMT result shows generator step

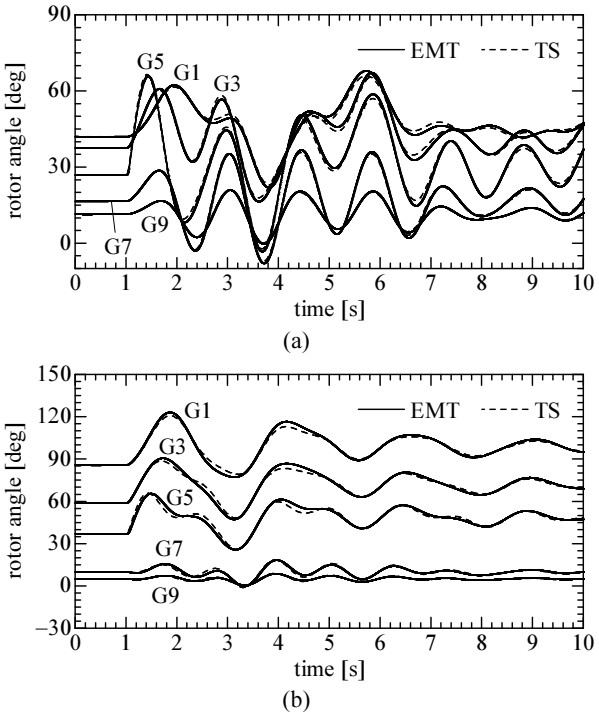

Fig. 6. EMT simulation results of the cases where a 3LG fault occurs at F. The rotor angles of G1, G3, G5, G7, and G9 are shown. (a) Peak-load condition. (b) Light-load condition. The TS simulation results for the same cases are superimposed by dashed lines.

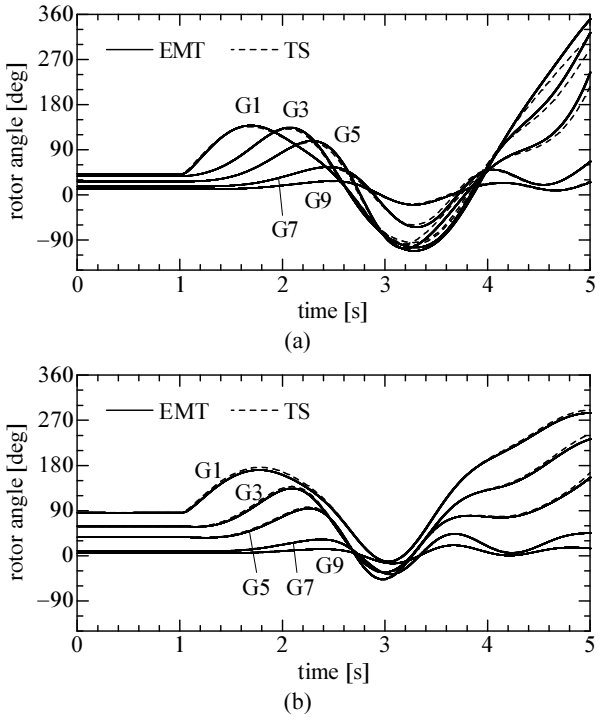

Fig. 5. EMT simulation results of the cases where a 3LG fault occurs at A. The rotor angles of G1, G3, G5, G7, and G9 are shown. (a) Peak-load condition. (b) Light-load condition. The TS simulation results for the same cases are superimposed by dashed lines.

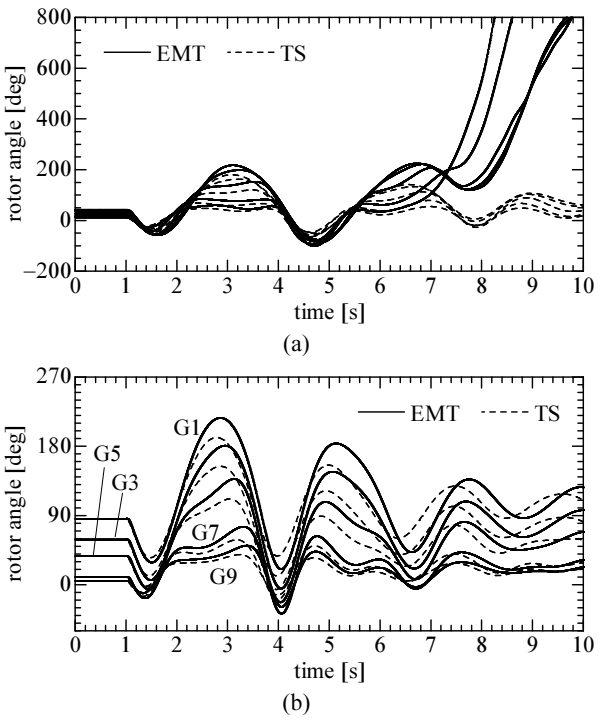

Fig. 7. EMT simulation results of the cases where a 3LG fault occurs at J. The rotor angles of G1, G3, G5, G7, and G9 are shown. (a) Peak-load condition (generators not identified since too crowded). (b) Light-load condition. The TS simulation results for the same cases are superimposed by dashed lines.

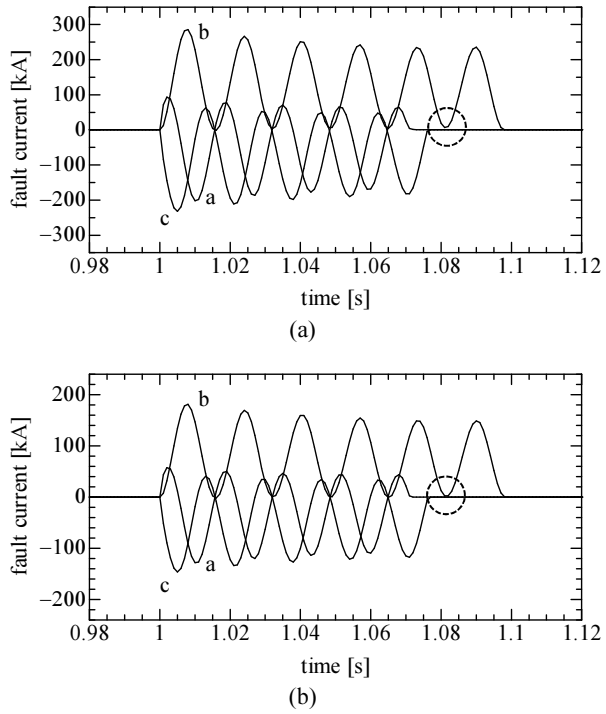

Fig. 8. Fault-current waveforms in the cases where a 3LG fault occurs at Point J. (a) Peak-load condition. (b) Light-load condition. Current zero missing is marked by dashed circles.

out, while the TS result does not. To investigate the cause of this discrepancy, the fault-current waveforms of the EMT results in these cases are shown in Fig. 8. In EMT simulations, a circuit breaker cannot turn off if its current does not cross zero due to a dc component. This phenomenon is called current zero missing. In Fig. 8, current zero missing occurs as marked by the dashed circles, since the currents of phase b do not cross zero at around $t = 1.07$ s. Due to the current zero missing, the fault duration time of phase b becomes longer than 70 ms in these EMT simulation cases, and this gives the results different from those of the corresponding TS simulations.

V. Impact of Line Modeling

To investigate the impact of line modeling, all transmission lines in the West-10 Benchmark System are now represented by the constant-parameter line model [9]. It takes into account traveling waves and coupling among wires. Since the wire arrangement of the 500-kV transmission lines is not given in the West-10 Benchmark System, the wire arrangement shown in Fig. 9 is assumed to calculate the line constants.

This wire arrangement can be considered a typical one for 500-kV transmission lines in Japan. Since 500-kV transmission lines in Japan are generally not transposed, the line constants were calculated as an untransposed line. To obtain the corresponding TS simulation results, each of the transmission lines is represented by ten sections of cascaded π equivalents to gain accuracy. Since the line constants used in the EMT simulations and those used in the TS simulations are not exactly the same, a slight difference is observed in the initial power-flow solutions in the results presented below.

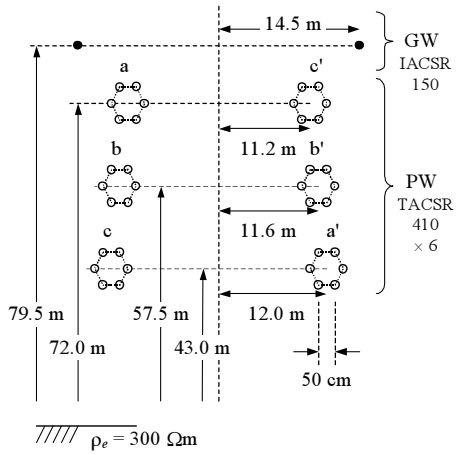

Fig. 9. Wire arrangement of the 500-kV transmission lines assumed for representation by the constant-parameter line model.

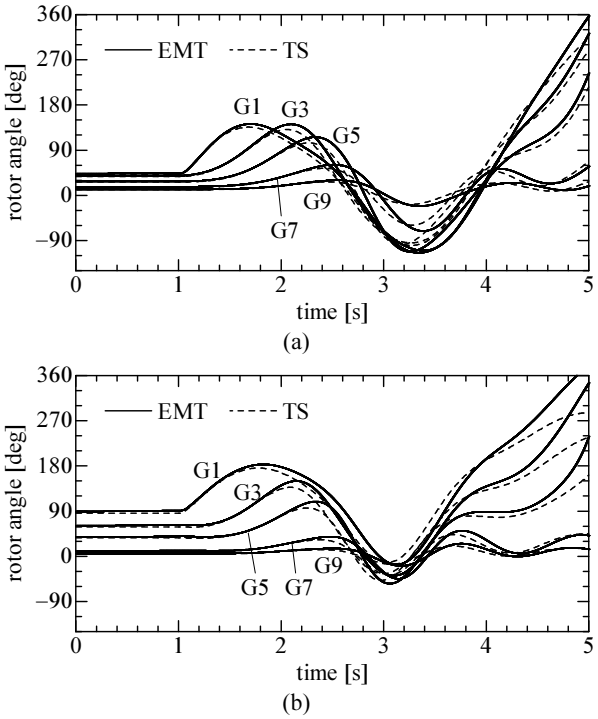

Fig. 10. EMT simulation results with the constant-parameter line model. Cases where a 3LG fault occurs at A. The rotor angles of G1, G3, G5, G7, and G9 are shown. (a) Peak-load condition. (b) Light-load condition. The TS simulation results for the same cases are superimposed by dashed lines.

Figs. 10, 11, and 12 show the simulation results when the 3LG fault mentioned in Section IV occurs at A, F, and J, shown in Fig. 1, respectively. Although a slight difference is observed in the initial power flow, the EMT simulation results agree well with the corresponding TS simulation results in the cases where the fault occurs at A and F. When the fault occurs at J in the peak-load condition, one of the generators steps out in the EMT result, while there is no generator stepping out in the TS result. Fig. 13 shows the fault-current waveforms of the EMT results when the fault occurs at J, and current zero missing is observed as marked by the dashed circle in the peak-load condition due to a large dc component. Apparently,

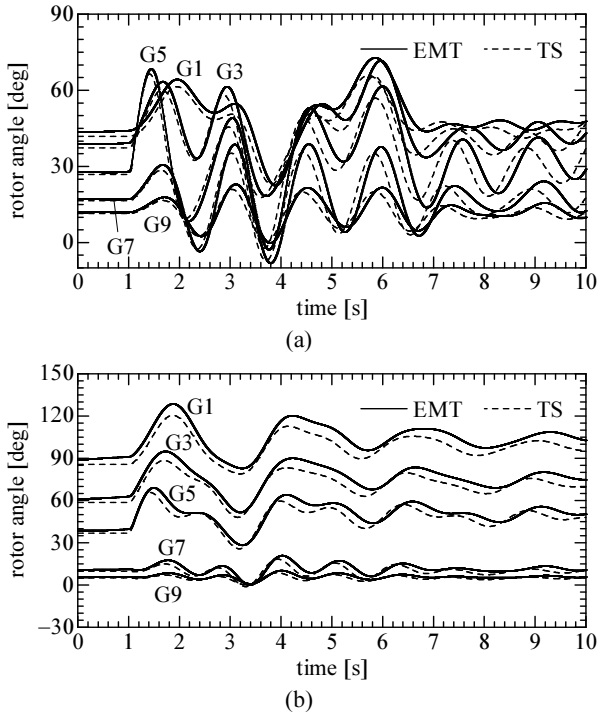

Fig. 11. EMT simulation results with the constant-parameter line model. Cases where a 3LG fault occurs at F. The rotor angles of G1, G3, G5, G7, and G9 are shown. (a) Peak-load condition. (b) Light-load condition. The TS simulation results for the same cases are superimposed by dashed lines.

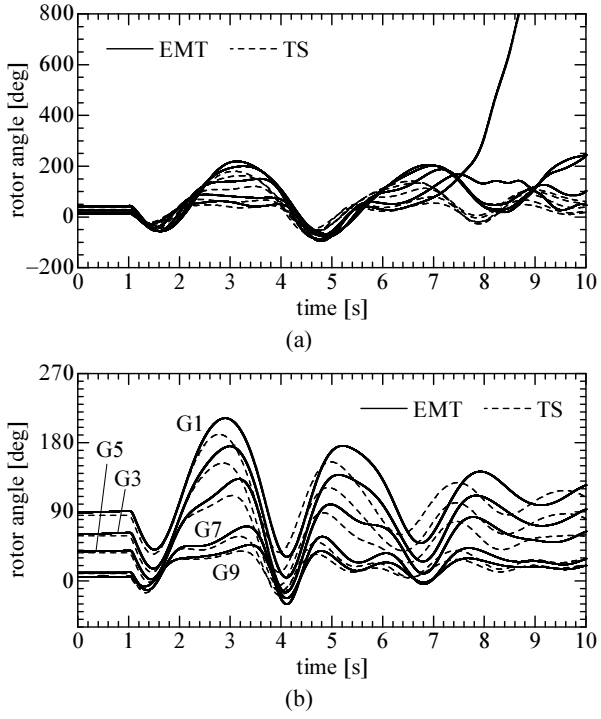

Fig. 12. EMT simulation results with the constant-parameter line model. Cases where a 3LG fault occurs at J. The rotor angles of G1, G3, G5, G7, and G9 are shown. (a) Peak-load condition (generators not identified since too crowded). (b) Light-load condition. The TS simulation results for the same cases are superimposed by dashed lines.

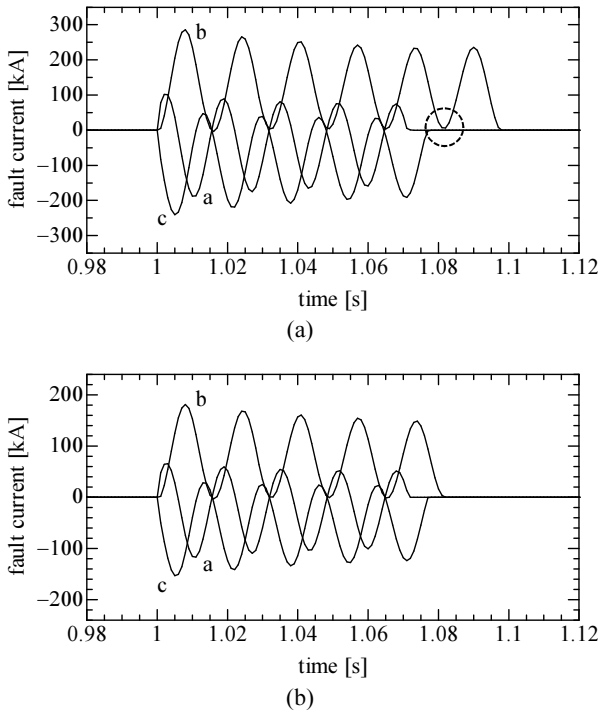

Fig. 13. Fault-current waveforms in the cases where a 3LG fault occurs at Point J, obtained with the constant-parameter line model. (a) Peak-load condition. (b) Light-load condition. Current zero missing is marked by a dashed circle.

the discrepancy comes from this current zero missing, and this discussion is similar to that in Section IV.

It may be concluded from the simulation results shown above that line modeling does not have a significant impact on simulation results of system-wide studies, when balanced fault conditions such as 3LG are applied. Further studies should be undertaken to investigate the impact for unbalanced fault conditions. Use of a frequency-dependent line model for more realistic transmission-line representation may be an interesting future study.

VI. Conclusion

In this paper, the West-10 benchmark power system model prepared by the Institute of Electrical Engineers of Japan (IEEJ) has been expanded and converted to an EMT model for the implementation in electromagnetic transient (EMT) simulation programs. Using the developed EMT model of the West-10 benchmark power system, simulations with various fault scenarios have been carried out. In most cases, the results obtained by the EMT model agree well with those obtained by the original transient stability (TS) model. It has been found that when the dc components of fault currents are large, the results obtained by those two simulation methods are different due to current zero missing of circuit breakers. It should be noted that we cannot conclude which method is correct, since a circuit breaker may be able to interrupt a residual current fairly close to zero (although current zero is missed). The impact of line modeling for balanced fault conditions has also been studied.

REFERENCES

[1] Committee for Standardization of Benchmark Power System Models, "Standard benchmark power system models," *IEEJ Technical Report*, no. 754, 1999 (title translated into English by the authors).

[2] Power System Stability Study Group, "Integrated analysis software for bulk power system stability," *CRIEPI Report*, no. T14, Apr. 1990.

[3] T. Noda, "International and domestic development trends of electromagnetic transient analysis programs for power systems," *IEEJ Trans., Power and Energy*, vol. 131, no. 11, pp. 872–875, 2011.

[4] T. Noda, K. Takenaka, and T. Inoue, "Numerical integration by the 2-stage diagonally implicit Runge-Kutta method for electromagnetic transient simulations", *IEEE Trans., Power Delivery*, vol. 24, no. 1, pp. 390–399, Jan. 2009.

[5] T. Noda, T. Kikuma, and R. Yonezawa, "Supplementary techniques for 2S-DIRK-based EMT simulations" *Electric Power Systems Research*, vol. 115, pp.87–93, Oct. 2014.

[6] T. Noda and T. Kikuma, "A robust and efficient iterative scheme for the EMT simulations of nonlinear circuits," *IEEE Trans., Power Delivery*, vol. 26, no. 2, pp. 1030–1038, Apr. 2011.

[7] T. Noda and K. Takenaka, "A practical steady-state initialization method for electromagnetic transient simulations," *Proc., IPST 2011*, paper # 99, Delft, The Netherlands, 2011.

[8] O. Sakamoto, T. Nakajima, H. Takizawa, T. Noda, and K. Takenaka, "Development of a synchronous machine model considering simplified saturation of the interlinkage magnetic flux behind the armature winding leakage inductance for XTAP," *Proc., IEEJ Technical Meeting on Rotating Machinery*, paper # RM-13-118, Sendai, Japan, 2013.

[9] H. W. Dommel, "Digital computer solution of electromagnetic transients in single- and multi-phase networks," *IEEE Trans., Power Apparatus and Systems*, vol. PAS–88, no. 4, pp. 388–399, Apr. 1969.